Open access • Journal Article • DOI:10.1002/ANIE.201906870

Defect-Rich Graphene Nanomesh Produced by Thermal Exfoliation of Metal-Organic Frameworks for the Oxygen Reduction Reaction. — Source link

Wei Xia, Jing Tang, Jingjing Li, Shuaihua Zhang ...+4 more authors

Institutions: Nanjing University of Aeronautics and Astronautics, East China Normal University, National Institute for Materials Science, National Taiwan University ...+1 more institutions

Published on: 16 Sep 2019 - Angewandte Chemie (Wiley)

Topics: Nanomesh and Graphene

Title: Defective Graphene Nanomesh Produced by Thermal Exfoliation of Metal-Organic Frameworks

Authors: Wei Xia; Jing Tang; Jingjing Li; Shuaihua Zhang; Chia-Wen Wu; Jianping He; Yusuke Yamauchi

To be cited as: 10.1002/anie.201906870

Link to VoR: https://doi.org/10.1002/anie.201906870

Defective Graphene Nanomesh Produced by Thermal Exfoliation of Metal-Organic Frameworks

Wei Xia[+a,c], Jing Tang[+*b], Jingjing Li[a], Shuaihua Zhang[c], Chia-Wen Wu[d], Jianping He[a*], and Yusuke Yamauchi[e*]

Abstract: Two-dimensional (2D) materials usually exhibit extraordinary performance in lots of applications. Although graphene nanomesh is quite attractive as a member of 2D carbon materials, general synthetic routes to produce functional graphene nanomesh in large-scale are complex and tedious. Here, we elaborately design a simple two-step dimensional reduction strategy for exploring nitrogen-doped graphene nanomesh by thermal exfoliation of crystal- and shape-modified metal–organic frameworks (MOFs). MOF nanoleaves with 2D rather than 3D crystal structure is used as the precursor, which are further thermally unraveled into nitrogen-doped graphene nanomesh by using metal chlorides as the exfoliators and etching agent. Surprisingly, the prepared nitrogen-doped graphene nanomesh shows a unique ultrathin two-dimensional morphology, high porosity, rich and accessible nitrogen-doped active sites, and defective graphene edges, contributing to an unprecedented catalytic activity for oxygen reduction reaction in acid electrolytes. This approach is suitable for scalable production and is probably universal for synthesis of thousands of novel low-dimensional functional carbon materials by breaking the dimensional limitation of traditional three-dimensional MOFs and further executing thermal exfoliation.

Introduction

Among series of two-dimensional (2D) materials [1], the widely identification of graphene nanomesh (GM), i.e., porous graphene, is a relatively new concept of two-dimensional single- or few-layer of carbon nanosheet with in plane nanopores [2]. In contrast to perfect graphene nanosheets which are prone to aggregate, GM have increased specific surface areas and accessible vertical pathway between the layers, which expand the application of GM in energy related systems [3]. For example, the numerous nanoholes endow GMs with lots of defective edges, which probably provide extra active sites for catalyzing oxygen reduction reaction (ORR) [4]. To date, the most convenient method to produce large-scale GM is pore engineering of reduced graphene oxide (GO) to create nanopores and defect in the basal planes, including chemical activation of graphite oxide [5]. Therefore, a general route to produce catalytic active GM in large-scale will include preparation of GO precursor (e.g., via chemical exfoliation of graphite), pore engineering of GO, and post-doping of heteroatoms, which is quite tedious and lack of novelty.

Recently, one-step carbonization of metal-organic frameworks (MOFs) [6] have become the most convenient method for preparing functional heteroatoms- and/or metal-doped carbon [7]. Is it possible to prepare functional GM in large scale via simply carbonization of easily obtained MOF precursor? Although it was considered as an advantage that MOF-derived carbon would inherent the shape and porous characteristic from MOF parent, we find it becomes a bottleneck to prepare MOF-derived carbons with low dimensions. Because most of the existed MOFs that can be prepared under mild conditions via simple processes have three-dimensional (3D) crystal structure and shape. Recently, Xu's group synthesized rod-shape MOF-74 instead of common microcrystalline MOF-74 by addition a modulator (salicylic acid). Then preparing one-dimensional carbon nanorods by thermal transform of rod-shaped MOF-74 [8]. It is inspiring that breaking the dimensional limitation of traditional 3D MOF probably pave the pathway to prepare novel low-dimensional MOF-derived carbon.

As a representative example, we find that the horizon of 3D zeolite imidazolate framework (ZIF) nanoparticles can be expanded to ZIF nanoleaves with 2D crystal structures and 2D shape by simply replacing the methanolic solvent with water. In details, 2-methylimidazole served as a bidentate bridging ligand that uses two N atoms to coordinate with metal ions to form zigzag chain units (**Scheme 1**). Each chain is hydrogen bonded to form an overall 2D supramolecular frameworks [9a]. Inspired by the unique layered structure and N-containing organic links of ZIF nanoleaves, we attempt to unravel the impact layers for preparing N-doped graphene nanomesh (NGM).

Herein, ultrathin NGM was fabricated successfully by an elaborately designed two-step dimensional reduction strategy. Zn-containing ZIF nanoleaves (Zn-ZIF-L) with 2D crystal structure rather than regular ZIF with 3D structure was first selected as the precursor. Then Zn-ZIF-L was further exfoliated into ultrathin 2D NGM under inert atmosphere by using metal chlorides as the

a. *College of Materials Science and Technology, Jiangsu Key Laboratory of Materials and Technology for Energy Conversion, Nanjing University of Aeronautics and Astronautics, 210016 Nanjing, China*
E-mail: jianph@nuaa.edu.cn
b. *School of Chemistry and Molecular Engineering, Shanghai Key Laboratory of Green Chemistry and Chemical Processes East China Normal University, Shanghai 200062, China*
E-mail: jingtang@chem.ecnu.edu.cn
c. *International Center for Materials Nanoarchitectonics (MANA), National Institute for Materials Science (NIMS), 1-1 Namiki, Tsukuba, Ibaraki 305-0044, Japan*
d. *Chemical Engineering, National Taiwan University, No. 1, Sec. 4, Roosevelt Road, Taipei 10617, Taiwan*
e. *School of Chemical Engineering and Australian Institute for Bioengineering and Nanotechnology (AIBN), The University of Queensland, Brisbane, Queensland 4072, Australia*
E-mail: y.yamauchi@uq.edu.au
\+ *These authors contribute equally to the work*

exfoliators and etching agent. The best NGM shows a quite thin thickness (1.3 nm), a high specific surface area (1329.5 m^2 g^{-1}), nitrogen doping (4.68 at%) as well as abundant hierarchical porous structure. Thanks to the overall structural and compositional advantages, NGM exhibits an unprecedented catalytic activity for ORR in acid electrolyte, which make a great breakthrough in metal-free carbon-based catalyst for acidic ORR.

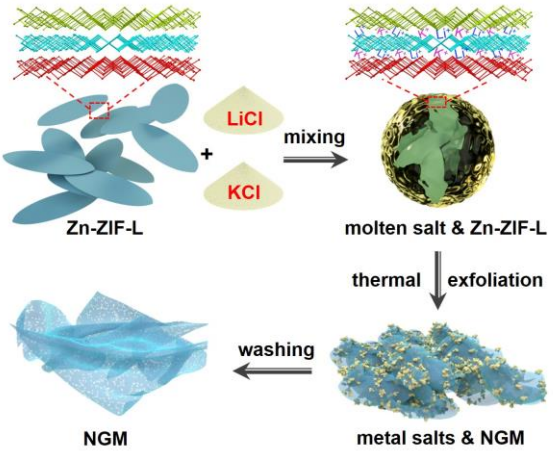

Scheme 1. *Illustration of thermal exfoliation of Zn-ZIF-L to produce NGM.*

Results and Discussion

Zn-ZIF-L was first prepared by using zinc nitrite and 2-methylimidazole precursors in aqueous solution. Zn-ZIF-L shows a leaf-like shape, a thickness of ~160 nm, and a lateral dimensional size of ~ 5 μm (**Figure S1a**). The layered crystal structure of Zn-ZIF-L is simulated in **Scheme 1** based on the experimental X-ray diffraction (XRD) pattern, which matches well with simulated XRD pattern of Zn-ZIF-L (**Figure S1b**) [9]. Direct carbonization of Zn-ZIF-L at typical temperature of 800 °C produces a leaf-like nitrogen-doped porous carbon (NC-L-800) with a bit distorted shape (**Figure S2**) compared with the original Zn-ZIF-L precursor (**Figure S1a**). In order to unravel the impact crystal layers of Zn-ZIF-L and produce Zn-ZIF-L derived 2D ultrathin porous carbon, exfoliator and etching agent of LiCl/KCl was used and mixed with Zn-ZIF-L precursors adequately (**Scheme 1**). Then, the mixture was heat treated under the protection of nitrogen atmosphere from room temperature to maximum 900 °C to produce nitrogen-doped graphene nanomesh (NGM). As monitored by the TGA-DSC analysis (**Figure S3a**), the mixture shows a pronounced endothermic process at 369 °C which corresponds to the melting of LiCl/KCl [10]. Another two endothermic process at 509 °C and 684 °C might due to the slight compositional change of Zn-ZIF-L [11]. Although the weight of Zn-ZIF-L might change a bit, the molten metal chlorides are quite stable below 700 °C [12]. Therefore, the total weight seems constant below 700 °C considering that the content of Zn-ZIF-L is only ~2wt% in the mixture. After the temperature is increased to more than 700 °C, the mixture starts to lose weight accompanying with an obvious endothermic peak at 859 °C, which might due to the strong interaction between Zn-ZIF-L and LiCl/KCl accompanied with exfoliation, carbonization, and volatile of decomposed chemicals. In addition, vaporization of LiCl/KCl molten salts also happens when the temperature reaches to 800 °C [12] and contribute to the fast weight loss. In contrast, pyrolysis of individual Zn-ZIF-L shows a totally different TG/DSC curve that shows much simpler process (**Figure S3b**). Based on the TGA-DSC analysis and the morphology observation of Zn-ZIF-L before (**Figure S1a**) and after (**Figure S4a,b**) thermal treatment, we propose the following reaction process (**Scheme 1**). When the LiCl/KCl is molten (> 369 °C), the small metal ions would insert into the crystal layers. Then, the exfoliation, carbonization, and evaporation would happen simultaneously at the higher temperatures (> 700 °C). After cooling down, the 2D ultrathin nitrogen-doped porous carbon nanosheets contain metal salts and other impurities (**Figure S4a**). These impurities are proved to be Li_xC_y and $LiKCO_3$ according to the XRD patterns (**Figure S4c**), but they can be fully removed by washing with acid. Finally, the product of nitrogen-doped graphene nanomesh (NGM) was obtained. Traditional Zn-ZIF polyhedron with 3D crystal structure (**Figure S5a-b**) was also thermally treated by the same process. However, irregular carbons without sheet-like morphology were obtained (**Figure S5c-d**). Even though metal ions (Li^+ and K^+) inserted into the cavities of 3D Zn-ZIF, it is difficult to unraveling the interconnected 3D crystal structure and converting into 2D layered carbons.

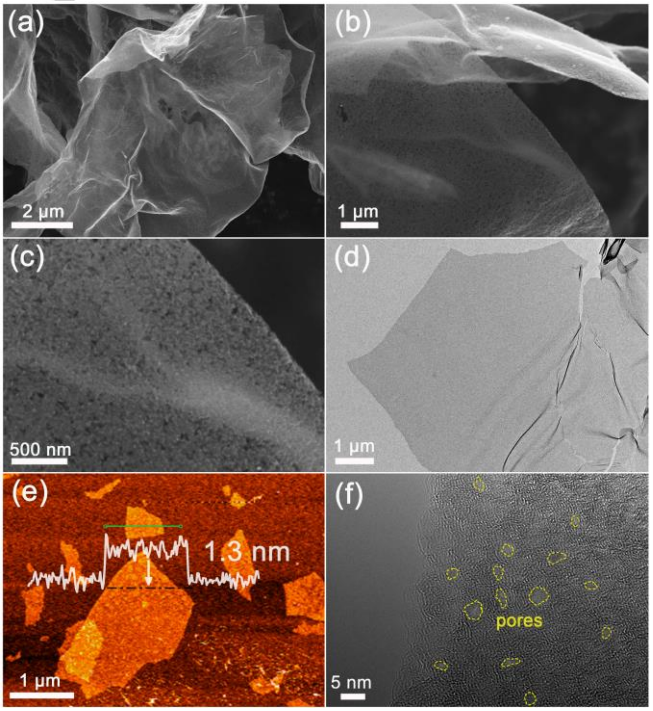

Figure 1. *(a-c) SEM images, (d) TEM image, (e) AFM image, and (f) HRTEM image of NGM-800 (yellow cycle indicates the nanopore).*

As observed from the scanning electron microscopy (SEM) image, NGM prepared at 800 °C is composed of ultrathin nanosheets with lateral sizes reach up to a few micrometers (**Figure 1a-b and Figure S6a**). Massive nanopores can be observed clearly on the surface of NGM nanosheet (**Figure 1c and Figure S6b,c**). As shown in **Figure 1d** and **Figure S7a**, transmission

electron microscopy (TEM) images also prove a transparent nanosheet, indicating the quite thin NGM. The thickness of NGM was carefully estimated by atomic force microscope (AFM), which is approximately 1.3 nm (**Figure 1e**). Furthermore, high-resolution TEM image reveals that NGM mainly consists of a few layered graphene sheets ('defective' graphitic carbon) as well as nanoporous structure (**Figure 1f and Figure S7b,c**). Metal elements (e.g. K, Li, Zn) and other impurities (e.g. Cl) is hardly detected by EDX (**Figure S8a**). Elemental mappings of NGM clearly show the homogeneously distributed nitrogen, carbon, and oxygen (**Figure S8b**).

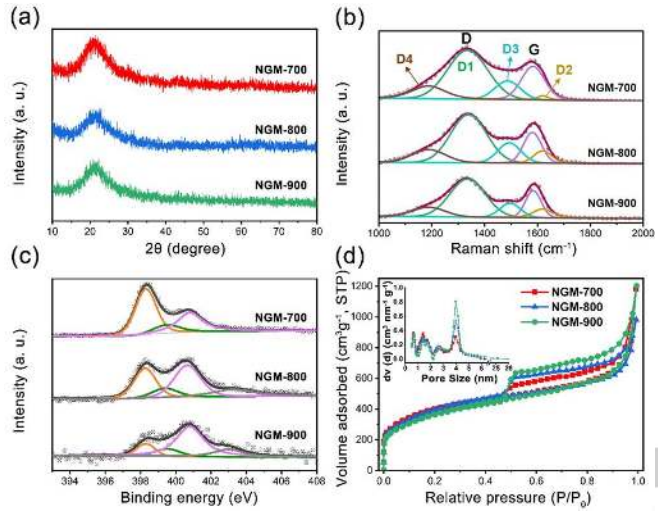

Figure 2. *(a) XRD patterns, (b) Raman spectra, (c) high-resolution N 1s XPS spectra, and (d) N_2 adsorption-desorption isotherms of NGM-x (x=700, 800, 900). Pore-size distributions are inset in (d).*

For studying the influence of temperature on the structural properties of NGM, we conducted different thermal exfoliation at 700 to 900 °C in case of excess weight loss. The corresponding samples was named as NGM-*x* (*x*=700, 800, 900). According to the XRD analysis (**Figure 2a**), all the samples present a wide peak centered at ~21°, which can be attributed to the diffraction of (002) plane of low-graphitic carbon materials. However, the common (002) diffraction peak of amorphous carbon is usually observed at 25°, similar to that of NC-L-800 in **Figure S9a**. The peak shift of NGM-*x* towards lower angles indicates an expanded interlayer distance in the direction of (002) [13].

Raman spectra is useful to identify the disordered degree of carbon materials due to its sensitivity in the short-range ordered structure. The spectra (**Figure 2b** and **Figure S9b**) are fitted into five Raman bands (G, D1, D2, D3, D4) by using Gaussian–Lorentzian numerical simulation for all the samples (**Table S1**) [14], which are adopted to provide quantitative evidence for the degree of structural disorder in the first-order spectral region (1000 ~ 2000 cm^{-1}). Normally, G band located at ~1580 cm^{-1} is known to be features of perfect graphitic lattice, and D1 band corresponds to the vibration mode of carbon atoms at the graphene edges. Generally, the disordered degree of carbon can be estimated by the relativity of integrated areas of D1 to G band (I_{D1}/I_G). The calculated ratios of I_{D1}/I_G are 2.17 for NC-L-800, 2.35 for NGM-700, 3.15 for NGM-800, and 3.19 for NGM-900. The results show that I_{D1}/I_G increased after the extensive exfoliation at higher temperatures, indicating a much higher percentage of carbon atoms at the edges of graphene layer (as observed in **Figure 1f**), which are regarded as probable active sites for catalysis.

The element status of NGM-*x* (*x*=700, 800, 900) and NC-L-800 was investigated by X-ray photoelectron spectroscopy (XPS). As shown **Figure S10,** Li and K are not detected by XPS, indicating that the metal-containing impurities can be fully removed from final NGM-*x* by acid washing. The nitrogen contents in NGM-*x* (*x*=700, 800, 900) are estimated to be 11.54, 4.68, and 2.82 at%, respectively. The decrease content of N is reasonable considering the more extensive thermal exfoliation and carbonization at higher temperatures. The high-resolution N1s spectra (**Figure 2c and Figure S9c**) can be deconvoluted into four different bands which correspond to pyridinic N (~398.4 eV), pyrrolic N (399.5 eV), graphitic N (400.7 eV), and N^+-O species (402 ~ 405 eV) [15], respectively. The ratios of different kinds of N in NGM-*x* were summarized in **Table S2**. The graphitic N and pyridinic N species, which have been regarded as the active sites for ORR [16], account for more than 70 % in the total nitrogen in NGM-*x*. Although being treated at the same temperature, NGM-800 possess less nitrogen contents of 4.68 at% compared with NC-L-800 (14.88 at%). The strong thermal exfoliation process would severely etch the carbon frameworks, finally leading to a decreased nitrogen content and creating the nanopores and defects.

N_2 adsorption-desorption analysis was carried out to estimate the different porosities of NGM-*x* (*x*=700, 800, 900) and NC-L-800 samples. The parameters of pore structure are summarized in **Table S3**. The thermal exfoliation brings obvious changes on the pore structure and specific surface area of Zn-ZIF-L derived carbon materials. NGM-*x* (*x*=700, 800, 900) (**Figure 2d**) displayed a type-IV isotherms with more obvious hysteresis loop compared with NC-L-800 (**Figure S9d**), which reveals the characteristic of more distinct mesopores. The detail pore size distributions are shown in inset of **Figure 2d and Figure S9d**. NGM-*x* (**Figure 2d**) display higher N_2 adsorption at low relative pressure (P/P_0< 0.1) than NC-L-800 (**Figure S9d**), which accounts for the larger amount of micropores in NGM-*x* [5]. The specific surface area greatly increased from 682.7 $m^2\ g^{-1}$ for NC-L-800 to 1329.5 $m^2\ g^{-1}$ for NGM-800 after adopting the thermal exfoliation process instead of regular carbonization. It implies that the exfoliator of metal ions (K^+, Li^+) might insert into the layers of Zn-ZIF-L to unravel the layers to create more specific surface area, and further interact with carbon atoms to produce more micropores and mesopore during thermal exfoliation process [17]. In addition, the higher thermal exfoliation temperature leads to a decreased specific surface area, microporous structure, and total pore volume (**Table S3**) due to the excess exfoliation at high temperatures [5] as revealed by TG results (**Figure S3a**),

During the experiment, we find that the kinds of metal chlorides plays an important role during thermal exfoliation. As we discussed above, the metal ions (Li^+ and K^+) from molten metal chlorides probably inserted into the crystal layers of 2D Zn-ZIF-L

and unraveled the compact carbon layers during the thermal treatment. In this section, we would like to take a deep insight into the role of the exfoliators of KCl and LiCl. We tried to use the individual KCl or LiCl as the exfoliator, and the corresponding products obtained via thermal exfoliaiton at 800 °C was assigned as NGM-K and NGM-Li, respectively. We figure out that the K^+ and Li^+ ions play different roles during the thermal treatment. The mixed exfoliator consist of both KCl and LiCl is the key factor to produce NGM-800 (also labelled as NGM-mix in this section). As compared in **Figure 3a-b,** NGM-K is much thinner and smoother than NGM-Li. The NGM-Li nanosheets are thicker than NGM-K nanosheets, as roughly observed by SEM in **Figure S11a,c**, and there are richer pores on the surface of NGM-Li nanosheet (**Figure S11b,d**).

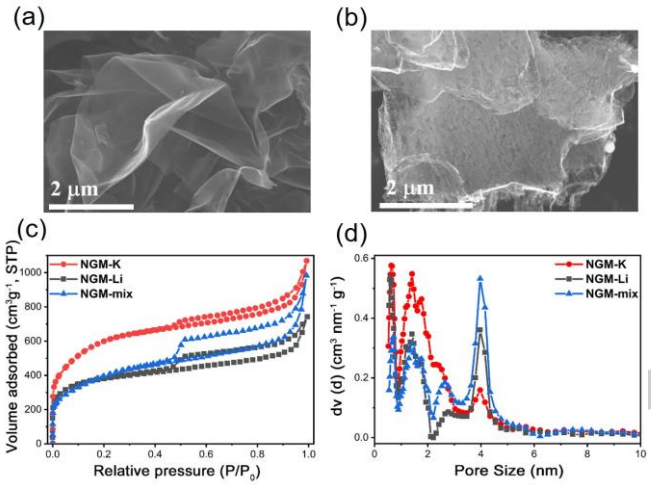

Figure 3. *SEM images of (a) NGM-K and (b) NGM-Li. (c) N_2 adsorption-desorption isotherms and (d) pore size distribution of NGM-K, NGM-Li, and NGM-mix (NGM-800) respectively.*

The different roughness are expected to bring a different porosity in NGM-Li and NGM-K. According to the N_2 adsorption-desorption isotherms (**Figure 3c**) and pore size distributions (**Figure 3d**), NGM-Li have a higher propotion of mesopores than NGM-K, which is in accordance with the rough and porous surface as observed by SEM images (**Figure 3b**). We suppose that although either K^+ or Li^+ is able to unravel the carbon layers, the K^+ ions are likely more effective in intercalation and exfoliation through intercalation-expansion-microexplosion in Zn-ZIF-L derived carbon. Thus, we guess that Li^+ ions might contribute more to etching the carbons to create larger mesopores (~4.0 nm). Therefore, after integrating the functionalities of KCl and LiCl, the mixed exfoliator produces the extraordinary NGM-mix (*i.e.* NGM-800) that consists of ultrathin nanosheets with a plenty of pores on the surface. The atomic scale defectives in NGM-mix will contribute to the formation of abundant active sites.

For considering real practical applications to fuel cell systems, metal-free catalysts with superior acidic ORR performance comparable to Pt are much desired. Dissolution of metal species really happens in practical harsh conditions (*e.g.*, high temperature, long term), causing serious reduction of ORR performance. Although the state of art metal-free carbon-based catalyst have comparable and even better performance for catalyzing ORR than commercial 20 wt% Pt/C in alkaline electrolyte (**Table S4**), they still show poor catalytic activity in acidic electrolyte. Thus, the ORR performances of NGM-*x*, NC-L-800, and Pt/C catalysts in 0.1 M $HClO_4$ solution were carefully studied.

Similar to the trend tested in alkaline electrolyte (**Figure S12-Figure S14**), NGM-800 showed the highest catalytic activity with the most positive ORR peak located at 0.68 V in acidic electrolyte (**Figure 4a**), which is much more positive than that of NGM-700 (0.44 V) and NGM-900 (0.65 V). As a metal-free carbon-based electrocatalyst, it is surprised that NGM-800 displays an unprecedented ORR activity with an impressive E_{onset} of 0.860 V, $E_{1/2}$ of 0.781 V, and J_d of 4.243 mA cm^{-2} (**Figure 4b**). Although the achieved performance is slightly inferior comparing to 20 wt% Pt/C which displays E_{onset} = 0.936 V, $E_{1/2}$ = 0.831 V, J_d = 5.246 mA cm^{-2}, it possesses the highest performance amongst metal-free carbon-based electrocatalysts reported to date (**Table S5**). In addition, kinetic current density (J_k) of NGM-800 calculated from **Figure 4b** is 38.12 mA cm^{-2} at 0.72 V, which is close to that of 20 wt% Pt/C (46.34 mA cm^{-2}) but is much higher than that of NGM-700 (0.59 mA cm^{-2}), NGM-900 (14.51 mA cm^{-2}), and NC-L-800 (≈ 0 mA cm^{-2}). The results demonstrate that porous ultrathin 2D structure significantly promotes the ORR kinetic process.

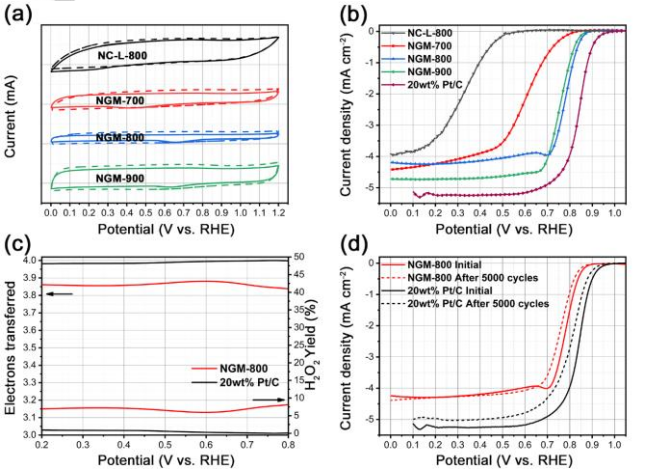

Figure 4. (a) CV curves of NGM-*x* (*x*=700, 800, 900) and NC-L-800 in O_2-saturated (solid line) or N_2-saturated (dashed line) 0.1 M $HClO_4$ at a scan rate of 50 mV s^{-1}; (b) LSV curves of NGM-*x* (*x*=700, 800, 900), NC-L-800, and 20 wt% Pt/C, (c) electron transfer number and peroxide yield of NGM-800 (red line) and 20 wt% Pt/C (black line) carried out in O_2-saturated 0.1 M $HClO_4$ at a scan rate of 5 mV s^{-1} under rotation speed of 1600 rpm; (d) LSV voltammograms of NGM-800 and 20 wt% Pt/C record in O_2-saturated 0.1 M $HClO_4$ before and after 5000 cycles.

The electron transfer number (n) for NGM-800 is calculated to be 3.85, and peroxide yield is below 7.6 % over potential range of 0.2 ~ 0.8 V (**Figure 4c**) based on the RRDE record in **Figure S15**. The results indicate that NGM-800 processed mainly a four-electron transfer pathway for ORR in acidic electrolyte, which was further demonstrated by Koutecky-Levich (K-L) plot derived from

LSV curves (**Figure S16**). In addition, NGM-800 catalyst is also stable in the acidic electrolyte. After carrying out 5000 continuous CV cycles, NGM-800 shows a small negative shift of $E_{1/2}$ = 23 mV with almost no decay of diffusion limiting current density (**Figure 4d**). In contrast, Pt/C showed a negative shift of $E_{1/2}$ = 36 mV and 3.6 % decay of diffusion limiting current density. The great catalytic of NGM-800 for acidic ORR are probably due to the ultrathin 2D morphology with hierarchical pores as well as defect-enriched structure. The unique low-dimensional and porous structure ensures the fast mass transport and sustainable exposure of active sites, and prevents the deactivation of active sites induced by the restacking of carbon nanosheets or the blocking of transfer pathways.

Conclusion

In summary, ultrathin nitrogen-doped graphene nanomesh (NGM) with outstanding electrocatalytic activity for ORR in acidic electrolyte was successfully prepared by simple and efficient thermal exfoliation of Zn-containing zeolite imidazolate framework nanoleaves (Zn-ZIF-L) under inert atmosphere by using the mixed KCl and LiCl as the exfoliators and etching agent. The effect of different metal chlorides on thermal exfoliaiton of Zn-ZIF-L was carefully investigated. We suppose that potassium ions are more effective in intercalation and exfoliation of Zn-ZIF-L derived carbon, whereas lithium ions might contribute more to etching the carbons to create larger mesopores. The prepared NGM shows unprecedented catalytic activity for ORR not only in alkaline but also in acid electrolytes due to its two-dimensional morphology with a thickness of 1.3 nm, a high specific surface area of 1329.5 m^2 g^{-1}, abundant nanopores and defective active sites. It is inspiring that breaking the dimensional limitation of tradition 3D MOF probably pave the pathway to prepare thousands of novel low-dimensional MOF-derived functional carbon materials and improve the performance in various applications.

Keywords: 2D materials • graphene nanomesh •thermal exfoliation • acidic oxygen reduction reaction

Acknowledgement

The authors wish to acknowledge Dr H. Kato and Dr H. Takahashi (Toyota Motor Corporation) for their effort to discuss our ORR performance.

References

[1] a) X. Chia, M. Pumera, *Nat. Catal.* **2018**, *1*, 909-921; b) M. Xu, T. Liang, M. Shi, H. Chen, *Chem. Rev.* **2013**, *113*, 3766-3798; c) C. Tan, X. Cao, X. Wu, Q. He, J. Yang, X. Zhang, J. Chen, W. Zhao, S. Han, G. Nam, M. Sindoro, H. Zhang, *Chem. Rev.* **2017**, *117*, 6225-6331; d) Y. Liu, C. Xiao, P. Huang, M. Cheng, Y. Xie, *Chem* **2018**, *4*, 1263-1283.

[2] T. G. Pedersen, C. Flindt, J. Pedersen, N. A. Mortensen, A. P. Jauho, K. Pedersen, *Phys. Rev. Lett.* **2008**, *100*, 136804.

[3] a) Y. Zhao, L. Qu, C. Hu, L. Song, L. Wang, G. Shi, L. Dai, L. Qu, *Energy Environ. Sci.* **2014**, *7*, 1913-1918; b) C. Tang, H. Wang, X. Chen, B. Li, T. Hou, B. Zhang, Q. Zhang, M. M. Titirici, F. Wei, *Adv. Mater.* **2016**, *28*, 6845-6851.

[4] a) W. Yuan, Y. Zhou, Y. Li, C. Li, H. Peng, J. Zhang, Z. Liu, L. Dai, G. Shi, *Sci. Rep.* **2013**, *3*, 2248; b) S. Banerjee, J. Shim, J. Rivera, X. Jin, D. Estrad, V. Solovyeva, X. You, J. Pak, E. Pop, N. Aluru, R. Bashir, *ACS nano* **2013**, *7*, 834-843.

[5] a) Y. Zhu, S. Murali, M. D. Stoller, K. J. Ganesh, W. Cai, P. J. Ferreira, A. Pirkle, R. M. Wallace, K. A. Cychosz, M. Thommes, D. Su, E. A. Stach, R. S. Ruoff, *Science* **2011**, *332*, 1537-154; b) F. Li, M. Xue, J. Li, X. Ma, L. Chen, X. Zhang, D. R. MacFarlane, J. Zhang, *Angew. Chem. Int. Ed.* **2017**, *56*, 14718-14722.

[6] a) K. S. Park, Z. Ni, A. P. Côté, J. Y. Choi, R. D. Huang, F. J. Uribe-Romo, H. K. Chae, M. O'Keeffe, O. M. Yaghi, Proc. *Natl. Acad. Sci. USA* **2006**, *103*, 10186-10191; b) H. Furukawa, K. E. Cordova, M. O'Keeffe, O. M. Yaghi, *Science* **2013**, *341*, 1230444.

[7] Y. V. Kaneti, J. Tang, R. R. Salunkhe, X. Jiang, A. Yu, K. C. W. Wu, Y. Yamauchi, *Adv. Mater.* **2017**, *29*, 1604898.

[8] P. Pachfule, D. Shinde, M. Majumder, Q. Xu, *Nat. Chem.* **2016**, *8*, 718-724.

[9] a) R. Chen, J. Yao, Q. Gu, S. Smeets, C. Baerlocher, H. Gu, D. Zhu, W. Morris, O. M. Yaghi, H. Wang, *Chem. Commun.* **2013**, *49*, 9500-9502; b) B. Motevalli, N. Taherifar, H. Wang, J. Z. Liu, *J. Phys. Chem. C* **2017**, *121*, 2221-2227.

[10] X. Liu, M. Antonietti, *Adv. Mater*. **2013**, *25*, 6284-6290.

[11] a) W. Ding, L. Li, K. Xiong, Y. Wang, W. Li, Y. Nie, S. Chen, X. Qi, Z. Wei, *J. Am. Chem. Soc.* **2015**, *137*, 5414-5420; b) W. Li, W. Ding, J. Jiang, Q. He, S. Tao, W. Wang, J. Li, Z. Wei, *J. Mater. Chem. A* **2018**, *6*, 878-883; c) Q. Lai, Y. Zhao, Y. Liang, J. He, J. Chen, *Adv. Funct. Mater.* **2016**, *26*, 8334-8344.

[12] W. Zhou, J. Zhang, *J. Alloy. Compd.* **2017**, *695*, 2306-2313.

[13] a) I. K. Moon, J. Lee, R. S. Ruoff, H. Lee, *Nat. Commun.* **2010**, 1, 73; b) J. Xu, L. Zhang, R. Shi, Y. Zhu, *J. Mater. Chem. A* **2013**, *1*, 14766-14772.

[14] a) X. Yao, Y. Ke, W. Ren, X. Wang, F. Xiong, W. Yang, M. Qin, Q. Li, L. Mai, Adv. Energy Mater. 2019, *9*, 1803260; b) A. Sadezky, H. Muckenhuber, H. Grothe, R. Niessner, U. Pöschl, *Carbon* **2005**, *43*, 1731-1742.

[15] a) S. Yang, X. Feng, X. Wang, K. Müllen, *Angew. Chem. Int. Ed.* **2011**, *50*, 5339-5343; b) L. Qie, Y. Lin, J. W. Connell, J. Xu, L. Dai, *Angew. Chem. Int. Ed.* **2017**, *56*, 6970-6974.

[16] a) D. Guo, R. Shibuya, C. Akiba, S. Saji, T. Kondo, J. Nakamura, *Science* **2016**, *351*, 361-365 ; b) N. Wang, B. Lu, L. Li, W. Niu, Z. Tang, X. Kang, S. Chen, *ACS Catal.*, **2018**, *8*, 6827-6836 ; c) J. Pampel, T. P. Fellinger, *Adv. Energy Mater.*, **2016**, *6*, 1502389.

[17] a) Z. Zhang, J. Sun, F. Wang, L. Dai, *Angew. Chem. Int. Ed.* **2018**, *57*, 9038-9043; b) L. Chen, G. Shi, J. Shen, B. Peng, B. Zhang, Y. Wang, F. Bian, J. Wang, D. Li, Z. Qian, G. Xu, G. Liu, J. Zeng, L. Zhang, Y. Yang, G. Zhou, M. Wu, W. Jin, J. Li, H. Fang, *Nature* **2017**, *550*, 380-383.

Table of Contents

Communications

A nitrogen-doped graphene nanomesh was simply prepared by thermal exfoliation of crystal- and shape-modified metal–organic frameworks. The obtained ultrathin nitrogen-doped graphene nanomesh with high porosity and defective graphene edges, showing an unprecedented catalytic activity for oxygen reduction reaction in acid electrolytes.

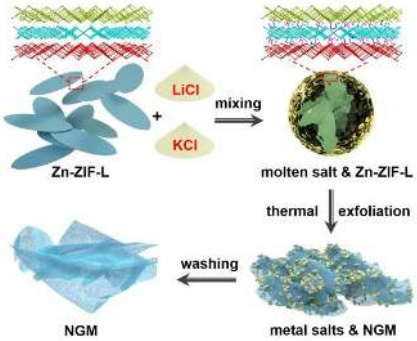

Wei Xia, Jing Tang, Jingjing Li, Shuaihua Zhang, Chia-Wen Wu, Jianping He* and Yusuke Yamauchi**

Page No. – Page No.

Defective Graphene Nanomesh Produced by Thermal Exfoliation of Metal-Organic Frameworks